

To appear in *Astronomical Journal*

UBVI and H α Photometry of the h & Persei cluster

Stefan C. Keller,

Institute of Geophysics and Planetary Physics,
Lawrence Livermore National Laboratory,
7000 East Ave., Livermore, CA 94550

skeller@igpp.ucb.edu

and

Eva K. Grebel

Max Planck Institute for Astronomy,
Königstuhl 17, D-69117 Heidelberg, Germany

ABSTRACT

UBVI and H α photometry is presented for 17319 stars in vicinity of the young double cluster h & Persei. Our photometry extends over a $37^0 \times 1^0$ field centered on the association. We construct reddening contours within the imaged field. We find that the two clusters share a common distance modulus of 11.75 \pm 0.05 and ages of $\log \text{age}(\text{yr}) = 7.1 \pm 0.1$. From the V-H colour, a measure of the H α emission strength, we conduct a survey for emission line objects within the association. We detect a sample of 33 Be stars, 8 of which are new detections. We present a scenario of evolutionary enhancement of the Be phenomenon to account for the peak in Be fraction towards the top of the main-sequence in the population of h & Persei and similar young clusters.

Subject headings: techniques : photometry Clusters : open (NGC 869, NGC 884) – Stars : evolution – emission-line, Be

1. Introduction

The double cluster h & Persei is one of the richest young galactic open clusters. The two clusters, h (NGC 869) and Persei (NGC 884) form the nuclei of the broader

Per OB 1 association (Morgan 1953). The region has been the focus of numerous studies. An extensive photographic study was presented by Osterho (1937); further photographic studies were made by Moat & Vogt (1974). Photometric studies were made by Johnson & Morgan (1955), Wildey (1964), Schild (1965) in Johnson UBV and by Crawford et al. (1970), Waelkens et al. (1990), Fabregat et al. (1996) and Marco & Bernabeu (2001) in Stromgren uvby. Infra-red photometry is presented by Tapia et al. (1984). A sample of proper motions is given in the central regions of h & Per. by Mumtaz (1983).

Given their relative richness and young age, these clusters form a useful comparison with stellar evolutionary models for massive stars. With MS populations up to $15M$ the clusters are analogous to the young populous clusters of the Magellanic Clouds. Within the literature, however, there is no convergence on the fundamental parameters of the clusters, such as their distances and ages. Marco & Bernabeu (2001) present distance modulus (dm) of 11.66 0.20 and 11.56 0.20 for h & Per. respectively. This is consistent with a common distance to the two clusters such as derived by Crawford et al. (1970): $dm = 11.4 \pm 0.4$ and Balona & Shobbrook (1984): $dm = 11.16$. Tapia et al. (1984) and Schild (1965) both find moduli of 11.7 and 12.0 for h & Per. respectively.

The age structure of the association has been discussed by Wildey (1964) and Schild (1967). Wildey concludes that a significant age spread is present within the larger Per OB 1 association with three notable epochs. Schild elaborates upon this, finding h to be older than Per. and discerns a third spatially diffuse population of yet younger age in the surrounding field. The present work revisits these issues in the light of our CCD-based photometry and the results of modern stellar evolutionary models.

Previous CCD-based studies have remained limited to the centralmost regions of the clusters. It is our goal in the present work to provide CCD-based photometry over an area broad enough to encompass the extent of the clusters. With this photometric basis we determine the fundamental parameters of the clusters: distance modulus, reddening (Section 4) and age (Section 6).

The presence of a large population of Be stars within the clusters has been noted by many authors (see e.g. Slettebak 1985 and Maeder et al. 1999). A Be star is a B-type star which has at some stage shown emission in H Balmer lines. This emission is understood to arise from an expelled circumstellar disk of material in the equatorial plane of the star. The mechanism for expulsion of this material is a topic of debate but is likely related to the generally rapid photospheric rotational velocity of the underlying star.

The means of Be star detection in these previous works has been through grism or long-slit spectroscopy. Such techniques, which have largely focused on the nuclei of the two

clusters, do not provide a sample with uniform completeness, especially for $V > 10$. Our study uses the $V - H$ colour index as a measure of the $H\alpha$ emission strength to distinguish the Be star population in a uniform manner throughout the observed field. The fraction of Be stars to total B stars within these clusters is a useful comparison with the Be star fractions observed within Magellanic Cloud clusters of similar ages (Keller et al. 2000). A recurring feature of the Be star population within young clusters is the peak in Be fraction towards the terminus of the main sequence. In Section 5 we discuss this feature and its implications for evolutionary modelling of the Be phenomenon.

2. Observations and Data Reduction

UBVI and $H\alpha$ photometry was performed on five nights between 17th and 25th of August 1999 at the San Diego State University Mount Laguna Observatory with the 1m telescope and a Loral 2048 \times 2048 CCD. The scale was 0.399 pixel $^{-1}$, yielding a field of view of 13.6° . Fifteen frame centers were taken to image the total field. The mosaiced 37°

field of our observations is shown in Figure 1.

The central wavelength and bandwidth of the $H\alpha$ filter were 6560 and 55Å respectively. Two sets of exposure times were used – long: 360 s in $H\alpha$, 300 s in U and 60 s in BV and I – and short: 40 s in U and I , 20 s in B , 10 s in V . The mean seeing for the observations was 1.08 . The observations were made in photometric conditions.

Preprocessing, such as overscan correction, bias subtraction and flat-fielding, was done using the IRAF CCDRED package. Instrumental magnitudes were obtained using DAOPHOT II via point-spread function fitting. The primary extinction coefficients and zeropoints were determined every night from observations of Landolt standard regions (Mark A, PG 1657+078, PG 2213-006, PG 1633+099; Landolt 1992). For the secondary extinction and transformation coefficients we used the mean of five independent determinations (errors represent the weighted mean errors). All the instrumental magnitudes were transformed to the standard UBVRI system using the following transformations:

$$V = v - k_{1,V} X + (0.006 \quad 0.007) (B - V) + v \quad (1)$$

$$B = b - k_{1,B} X - (0.021 \quad 0.004) (B - V) X - (0.053 \quad 0.004) (B - V) + b \quad (2)$$

$$U = u - k_{1,U} X + (0.011 \quad 0.005) (U - B) X - (0.120 \quad 0.013) (U - B) + u \quad (3)$$

$$I = i - k_{1,I} X + (0.063 \quad 0.012) (V - I) + i \quad (4)$$

where, following standard notation, k_1 , X and α represent the primary extinction coefficient, airmass and zeropoint respectively and the lowercase symbols denote the instrumental magnitudes. Table 1 lists the extinction coefficients and zeropoints. In the case of the H photometry only the effects of atmospheric extinction were accounted for. Table 2 presents our photometry.

The UBV magnitudes and colours from this study are compared with the previous photometry of WIlday (1964), Moore & Vogt (1974), Johnson & Morgan (1955), Kizisinski et al. (1999): NGC 864 nucleus and Kizisinski et al. (1997): NGC 884 nucleus) in Table 3. The number of stars used in the comparison is given in the fourth column by n_{tot} . Known variables were excluded in the statistics. The photographic photometry shows the largest scatter. The photometry of WIlday suffers greatly from the effects of crowding, this results in the large dispersion and generally brighter V magnitudes described in Table 3.

3. Photometric Diagrams

In Figure 2 we present the $U - B$, $B - V$ colour-colour (C-C) diagram from our photometry. In Fig. 2 a. we show the entire field. In panels b and c we show the C-C diagrams for h and Per. contained within the 10^0 radius. The choice of this radius for both clusters is made from examination of the radial object density around each cluster. At a radius of 10^0 the surface density diminishes to that of the background field.

The reddened zero-age main sequence (ZAMS) is also shown in Fig. 2 using the adopted distance moduli and mean reddening detailed in Sect. 4. The adopted ZAMS relation is from Balona and Shobbrook (1984). The dispersion seen about the mean MS locus (solid line) in Fig. 2 a. shows that there is significant differential reddening across the field.

Figures 3-5 show the $B - V$, $U - B$ and $V - I$ colour-magnitude (C-M) diagrams for the entire field, h and Per. respectively. Our photometry is saturated in B , V and I at 9.5. For stars brighter than $V = 9.5$ we have relied on previous photometry (Johnson & Morgan 1955; Hiltner 1956; WIlday 1964; Tapia et al. 1984). Points for which we have utilized one or more magnitudes from the literature are represented by triangular symbols in Figs. 2-5. Evolutionary departure from the ZAMS is seen in Figs. 4 and 3.

4. Reddening and Distance Moduli

We adopt the nominal values for colour-excess ratio $E(U - B) = E(B - V) = 0.72$ and the ratio of total to selective extinction, R ($A_V = E(B - V)$), of 3.2 (see e.g. Schmidt-Kaler

1982). Using those early M S, non-emission line stars ($U - B < 0.15$ and $B - V < 0.8$ in Figure 2) we derived $E(B - V)$ using the Q technique ($Q = (U - B) - 0.72(B - V)$; see e.g. Bessell 1991): $E(B - V) = (B - V)_{\text{obs}} - Q = 3.2$, where $(B - V)_{\text{obs}}$ is the observed colour.

In order to describe the spatially variable reddening our sample was divided into a grid of regions such that each region contained at least 10 stars for which we have determined $E(B - V)$. The resulting spatial distribution of $E(B - V)$ is shown in Figure 6. The region possesses a clear negative reddening gradient from SW to NE which is consistent with increasing galactic latitude. The nuclei of both clusters have average reddening of $E(B - V) = 0.54 \pm 0.02$ from 96 and 85 stars within h & Per. respectively. This is in agreement with the determination of Balona & Shobbrook (1984) from the UBV photometry of Crawford et al. (1970) of a mean reddening of $E(B - V) = 0.559 \pm 0.009$. Each star is then de-reddened on the basis of its position within Figure 6.

Once de-reddened, the ZAMS of Balona and Shobbrook (1984) was used to determine the distance modulus of each star. The bulk of the M S A & F stars ($V_0 = 12.5-15$) are well matched by the ZAMS. Significant evolutionary departures occur for the early B stars, these were excluded from our calculation. The distribution of distance modulus within the two clusters shows a broad peak centered at $V_0 - M_V = 11.75 \pm 0.05$. There is no significant difference in distance modulus of the two clusters. This result uses the bulk of the essentially unevolved M S. It is significantly more distant than the distance moduli derived by Balona & Shobbrook (1984) of $V_0 - M_V = 11.16 \pm 0.08$ which is derived from a limited sample of upper M S stars rectified to a similar sample of stars in the Pleiades. It is within the range of uncertainties of the Marco & Bernabeu (2001) result of $dm = 11.66 \pm 0.20$ and 11.56 ± 0.20 for h & Persei respectively.

5. The Be Star Population

For the purposes of selecting the population of emission-line objects we construct a $V, V - H$ C-M diagram (Fig. 7). We construct such a diagram in preference to the $V - I$, $V - H$ C-C diagram of previous studies (see Grebbeletal 1992 and Grebbe 1997). We find a total of 33 emission-line objects within the surveyed field as described in Table 4. The total from previous studies within this area is 25. Two known Be stars, Oo 566 and Oo 2262 were not found to exhibit significant emission on the epoch of our observations. We do not detect any faint emission-line objects which can be clearly associated with a pre-M S population.

6. Hertzsprung-Russell Diagram

6.1. Transformation to the H-R Diagram

In order to form the H-R diagram for the cluster populations we have made use of the model atmosphere broad-band colours, bolometric corrections and temperatures of Bessell, Castelli & Plez (1998). For stars of high effective temperature the UBV colours fail to provide good temperature indicators (Massey et al. 1995) and consequently we have used spectral types for temperature determination where possible for stars earlier than B2. These spectral types are drawn from Johnson & Morgan (1955), Schild (1965; 1967) and Slettebak (1968). In doing so we have used the spectral type - effective temperature conversion of Bohm-Vitense (1981). For later-type stars $(U - B) - T_{\text{eff}}$ and $(B - V) - T_{\text{eff}}$ relations were used with weights reflective of the temperature dependence to the colour of the star in question. Using the above relations the H-R diagram for h & Persei is constructed as shown in Figure 8.

6.2. Cluster Ages

In Figure 8 we have removed those stars which are highly likely to be non-members according to the proper motion study of Mumtaz (1983): with probability of membership less than 20%). Be stars were also excluded due to their anomalous colours produced by the presence of circumstellar material. This clarification is particularly useful in the vicinity of the MS turnoff. In Figure 8 we overlay stellar models by Bressan et al. (1993) and isochrones derived from them (Bertelli et al. 1994). The ages of the most massive stars lie between the isochrones of $\log \text{age}(\text{yr}) = 6.8$ and 7.2. Together with the evolved members the populations suggest a common age of $\log \text{age}(\text{yr}) = 7.1 \pm 0.1$ for the bulk of the population in both clusters, in line with the studies of Waelkens et al. (1990) and Denoyelle et al. (1990). This is in disagreement with the findings of Marco & Bernabeu (2001) who, from an examination of the average MS locus of both clusters, find that h Persei with a log age of 7.3 is older than Persei (with a log age of 7.0). Marco & Bernabeu go further to propose three epochs of star formation within h & Persei at log ages 7.0, 7.15 and 7.3. We propose that the analysis of Marco & Bernabeu (2001) is largely an over-interpretation of the available data. Our expanded dataset does not show any evidence for an age difference between the two clusters or multiple epochs of star formation.

It would be useful to consider the mass functions of the two clusters together with the age structure of the surrounding field. At present this is not possible. The existing proper motion study of Mumtaz (1983) is limited in magnitude ($V = 12$) and spatial extent (only the cluster cores are covered). There is no photometric method for distinguishing the cluster

members from members of the surrounding association due to the close a nity in age of the cluster and eld populations. Such analysis awaits more detailed proper motion studies.

7. The Be Star Fraction – Evidence for an Evolutionary Enhancement in Be Phenomenon?

In Figure 9 we present the Be fraction amongst M S B stars (to $M_V = +0.25$ – B9V Schmidt-Kaler 1982) within the eld of the association. The resulting distribution peaks at a fraction of 36% over the 0.5 mag. interval centered on $V_0 = 7.5$ which is in the vicinity of the M S turno for the association.

The peak in Be fraction seen at the M S turnus is also seen in several young clusters of the Magellanic Clouds (Keller et al. 2000 and Johnson et al. 2001). Yet studies of the Be fraction within the Galactic and LM C eld (see Zorec & Briot 1997 and Keller et al. 1999b respectively) show a more or less uniform proportion of around 15% over the spectral range B0-B5. To account for the observed difference in Be fraction between the cluster and eld environment we propose a scenario of evolutionary enhancement in the Be phenomenon. Our scenario utilises the one clear difference between the cluster and eld populations, namely the age spread within each population.

We consider a phase of enhancement of the Be phenomenon which occurs over an interval of the M S lifetime towards the end of the M S. The small age spread within the cluster population at the luminosity of the cluster M S turnus places the majority of the stars within the interval of Be enhancement. A peak in the Be fraction results at luminosities near the M S turnus and diminishes at lower luminosities as fewer stars reside within the age range of enhancement. At lower luminosities a population of Be stars remains. These stars are those with sufficient initial angular momentum to commence the Be phase. Within the eld population, which possesses a more uniform spread of ages for stars on the M S at a given mass, we see essentially the time-average of the proportion of Be stars. This is lower than that seen in the cluster and more-or-less uniform with luminosity.

The tendency for there to be a higher Be star fraction near the main-sequence turno is consistent with the rapid rotation hypothesis for Be star formation. The evolution of rotating stars has been examined by Endal & Soa (1979) and recently by Heger et al. (2000) and Meynet & Maeder (2000). These models explicitly follow the radialexchange of angular momentum with evolution. The quantitative details of the evolution of the equatorial surface velocity (v) depend critically on mass loss. Taking the example from Meynet & Maeder (2000), a $20M_\odot$ star with an initial v of 300 km s^{-1} drops to 120 km s^{-1} by the M S turno.

On the other hand a $12M_{\odot}$ star drops from 300 km s^{-1} to 200 km s^{-1} due to a substantially smaller mass loss rate. The evolution of $\frac{\omega}{\omega_{\text{crit}}}$, the surface angular velocity as a fraction of the critical angular velocity (i.e. the velocity at which the equatorial escape velocity drops to zero), is dependent on the treatment of redistribution of angular momentum within the stellar interior and of the effects of rotationally induced mixing. Heger et al. and Meynet & Maeder implement different treatments of the above but the qualitative conclusions are concordant: for stars less than $15M_{\odot}$, $\frac{\omega}{\omega_{\text{crit}}}$ increases towards the end of the MS lifetime.

Meynet & Maeder examine the case of a $20M_{\odot}$ star with a range of initial velocities. They find that the decrease in the surface ω is larger for larger initial velocities. This is due to the high stellar mass loss rates for rapid rotators. At lower masses we expect this behavior to be modified by lower mass loss rates. The models of Endal and Soa examine the rotational velocity evolution of a $5M_{\odot}$ star. They find that stars commencing their main-sequence lives with relatively slow angular velocity remain slow rotators throughout the whole of the main-sequence evolutionary phase (although there is a marked increase in angular velocity of all stars during the core contraction phase associated with exhaustion of hydrogen in the core, this evolutionary phase is far too short to account for the observed proportion of Be stars as was proposed by Schmidt-Kaler (1965) and recently by Bessell & Wood (1993). Thus slow rotators will never evolve into Be stars.

In contrast to the slow rotators, the models of Endal and Soa show that stars commencing their lives with an angular velocity greater than 56–76% of the critical breakup velocity ω_{crit} spin up to the critical velocity over a moderate fraction of the main-sequence lifetime. In a cluster where some fraction of the stars is formed with angular velocity greater than 50% of ω_{crit} , those stars nearer the main-sequence turnoff are more likely to be Be stars since they will have been more spun up by evolution than the less luminous stars that have not evolved as far through the main-sequence phase. This process could provide the mechanism of Be enhancement required to explain the concentration of Be stars to the main-sequence tip.

Numerous studies have indicated the importance of rotation within massive stars (e.g. Langer & Heger 2000 and Meynet & Maeder 2000). Rotationally induced mixing has been shown to be able to produce significant evolutionary and surface abundance changes. Observational evidence for the importance of rotation is growing, within $\text{h} \& \text{ Persei}$ in particular, the study of Vranden et al. (2000) provides a detailed chemical analysis of eight B1–B2 stars within the vicinity of the MS turnoff. They find, from the deduced HR diagram, a degree of extension to the end of the MS which is in agreement with evolutionary models which incorporate rotation.

8. Summary

We have obtained U B V I and H α photometry over a $37^0 \times 1^0$ field around the double cluster h & Persei. We have formed a spatial description of the reddening throughout the field. We have found that the clusters share a common distance modulus of 11.75 \pm 0.05 and possess ages of $\log \text{age}(\text{yr}) = 7.1 \pm 0.1$. Our study comprises a uniform survey for Be stars within the region. Using the V - H colour as a measure of the strength of H α emission we have identified 33 Be stars, 8 of which were previously unknown. The fraction of Be stars to total B stars shows a maximum at the end of the MS. Similar behaviour is seen in the Be population of young clusters in the Magellanic Clouds. This feature suggests an evolutionary enhancement in the Be phenomenon towards the end of the MS lifetime which we suggest is a consequence of rotational spin-up over the MS lifetime.

Work performed at LLNL is supported by the DOE under contract W-7405-ENG-48. The authors acknowledge the use of the WEBDA database maintained by J-C. Marillié, Univ. Lausanne. SCK acknowledges funding from the Australian Nuclear Science and Technology Organisation which made the observations possible. We thank Grant Miller of San Diego State University for assistance with the observing.

R E F E R E N C E S

Balona, L. A. & Shobbrook, R. R. 1984, MNRAS, 211, 375

Bertelli G., Bressan A., Chiosi C., Fagotto F., Nasi E., 1994, A&AS, 106, 275

Bessell, M. S., 1991, A&A, 242, L17

Bessell, M. S. & Wood, P. R. 1993, in New Aspects of Magellanic Cloud Research, 271

Bessell, M. S., Castelli, F. & Plez, B. 1998, A&A, 333, 231

Bohm-Vitense, E. 1981, ARA&A, 18, 241

Bressan A., Fagotto F., Bertelli G., Chiosi, C. 1993, A&AS, 100, 647

Crawford, D. L., Glaspey, J. W. & Perry, C. L. 1970, AJ, 75, 822

Denoyelle, J. et al. 1990, Ap&SS, 169, 109

Endal, A. S. & Soa, S. 1979, ApJ, 232, 531

Fabregat, J., Torrejón, J. M., Reig, P., Bemabeu, G., Busquets, J., Marco, A., & Reglero, V. 1996, A&AS, 119, 271

Grebel, E. K., Richter, T., & de Boer, K. S. 1992, A&A, 254, L5

Grebel, E. K. 1997, A&A, 317, 448

Heger, A., Langer, N. & Woosley, S. E. 2000, ApJ, 528, 368

Hiltner, W. A. 1956, ApJS, 2, 389

Johnson H. L., Morgan W. W. 1955, ApJ, 122, 429

Johnson R. A., Beaulieu, S. F., Gilmore, G. F., Hurley J., Santiago B. X., Tanvir N. R., Elson, R. A. W. 2001, astro-ph/0012389

Keller, S. C., Wood, P. R. & Bessell, M. S. 1999, A&AS, 134, 489

Keller, S. C., Bessell, M. S., & Da Costa, G. S. 1999 in IAU Coll. 175, ed. M. Smith, H. Henrichs & J. Fabregat (San Francisco: ASP), 141

Keller, S. C., Bessell, M. S., & Da Costa, G. S. 2000, AJ, 119, 1748

Krzesinski, J. & Pigulski, A. 1997, A&A, 325, 987

Krzesinski, J. & Pigulski, A. & Kolaczkowski, Z. 1999, *A & A*, 345, 505

Landolt, A. U. 1992, *AJ*, 104, 340

Maeder, A., Grebel, E. K. & Mermilliod, J.-C. 1999, *A & A*, 346, 459

Marco, A. & Bernabeu, G. 2001, *A & A*, accepted astro-ph/0102267

Massey, P., Lang, C., DeGioia-Eastwood, K. & Garmann, C. 1995, *ApJ*, 438, 188

Meynet, G. & Maeder, A. 2000, *A & A*, 361, 101

Moat, A. F. J. & Vogt, N. 1974, *Veroe. Astron. Inst. Bochum* 2

Morgan W. W. 1953, *ApJ*, 118, 318

Muminov M. 1983 *Bull. Inform. CDS*, 24, 95

Oosterhoff, P. T. 1937, *Ann. van de Sterrewacht te Leiden*, 17, 1

Schild, R. E. 1965, *ApJ*, 141, 979

Schild, R. E. 1967, *ApJ*, 148, 449

Schmidt-Kaler, T. 1965, *AJ*, 70, 691

Schmidt-Kaler, T. 1982, in Landolt-Bornstein, Vol 2, 23, eds. L. H. A. Liller et al. (2d ed.; Berlin: Springer-Verlag)

Slettebak, A. 1968, *ApJ*, 154, 933

Slettebak, A. 1985, *ApJS*, 59, 769

Tapia M., Roth M., Costero R. & Navarro S. 1984, *Rev. Mex. Astron. Astrofis.*, 9, 65

Vrancken, M., Lennon, D. J., Dufton, P. L., & Lambert, D. L. 2000, *A & A*, 358, 639

Waelkens, C. et al. 1990, *A & AS*, 83, 11

Wilden, R. L. 1964, *ApJS*, 8, 438

Zorec, J. & Briot, D. 1997, *A & A*, 318, 443

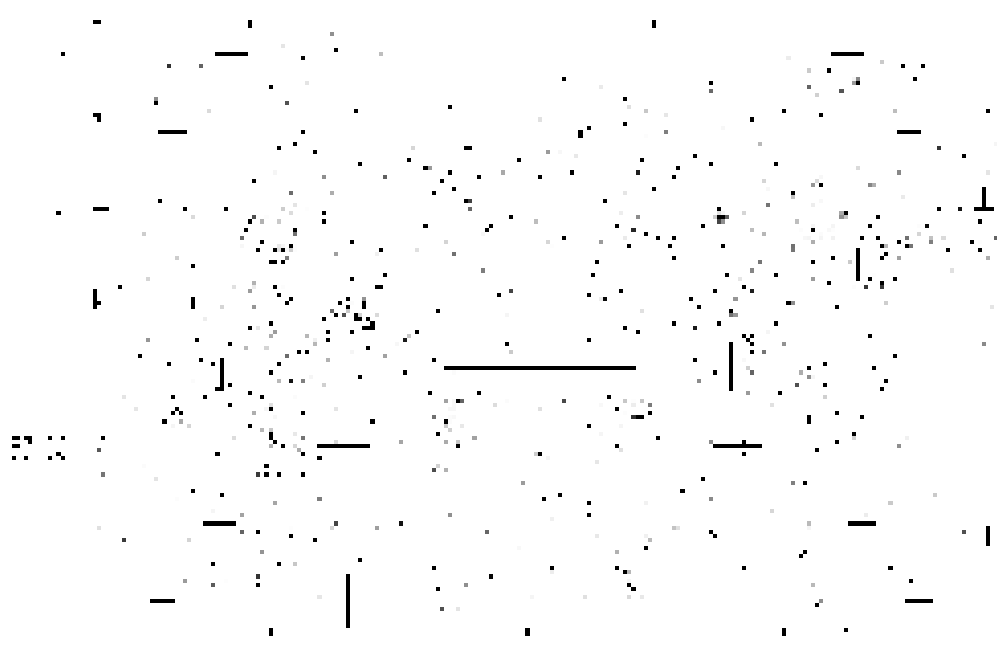


Fig. 1. | Mosaic of the field of the present study. The circles mark the boundaries taken for the extent of the individual clusters h (left) & (right) Persei as discussed below.

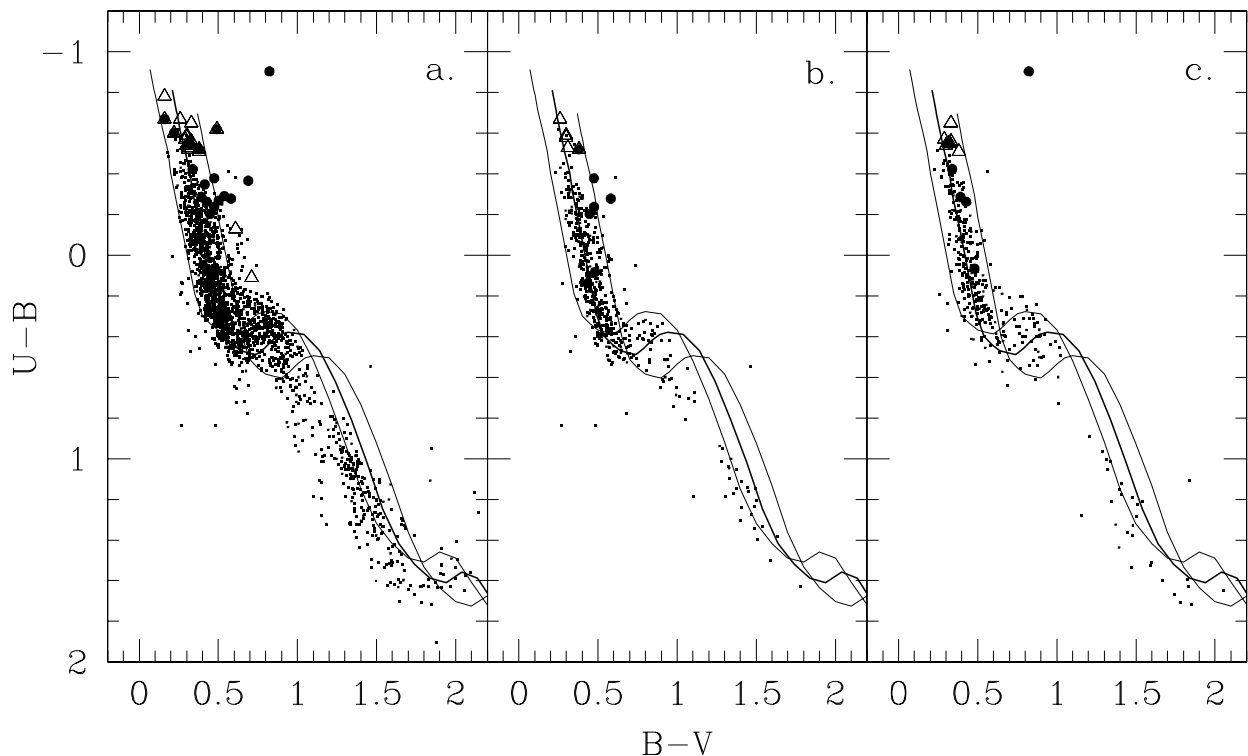


Fig. 2.1 U-B, B-V diagram for (a) the entire field (b) h Per. and (c) Per. The thick line represents the ZAMS relation for $E(B-V) = 0.54$, while the two thin lines are $E(B-V) = 0.65$ and 0.45 respectively. Filled circles are emission line stars and triangles are stars with photometry taken from the literature.

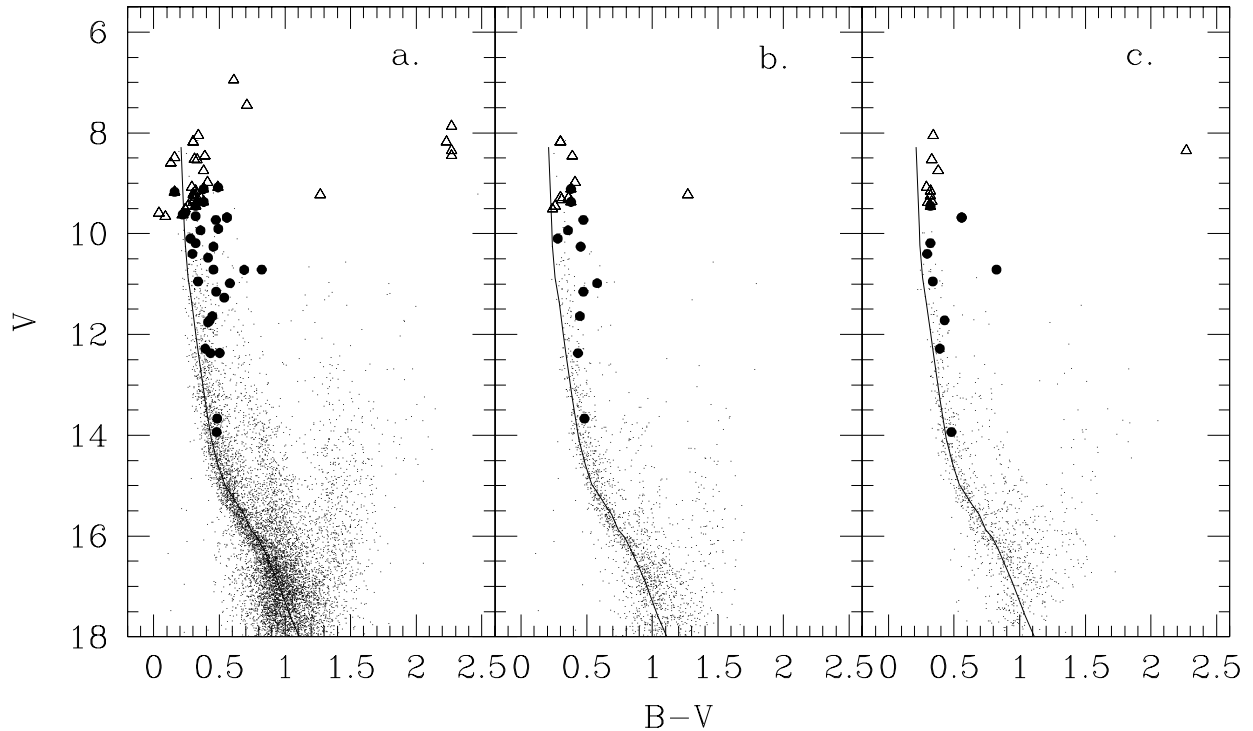


Fig. 3. | V , $B-V$ diagram. Symbols are as described in Figure 2. The thin line is the ZAM with $E(B-V) = 0.54$.

Date	$k_{1,V}$	$k_{1,B}$	$k_{1,U}$	$k_{1,I}$
Aug 17	0.147	0.015	0.142	0.021
Aug 18	0.135	0.011	0.158	0.042
Aug 19	0.150	0.017	0.145	0.025
Aug 21	0.138	0.025	0.152	0.031
Aug 23	0.159	0.031	0.163	0.022

Date	V	B	U	I
Aug 17	2.235	2.522	0.018	0.05
Aug 18	2.493	2.690	0.023	0.11
Aug 19	2.482	2.36	0.03	0.09
Aug 21	2.883	2.794	0.05	0.03
Aug 23	2.539	2.473	0.024	0.13

Table 1: Atmospheric extinction coefficients and photometric zeropoints from the present study

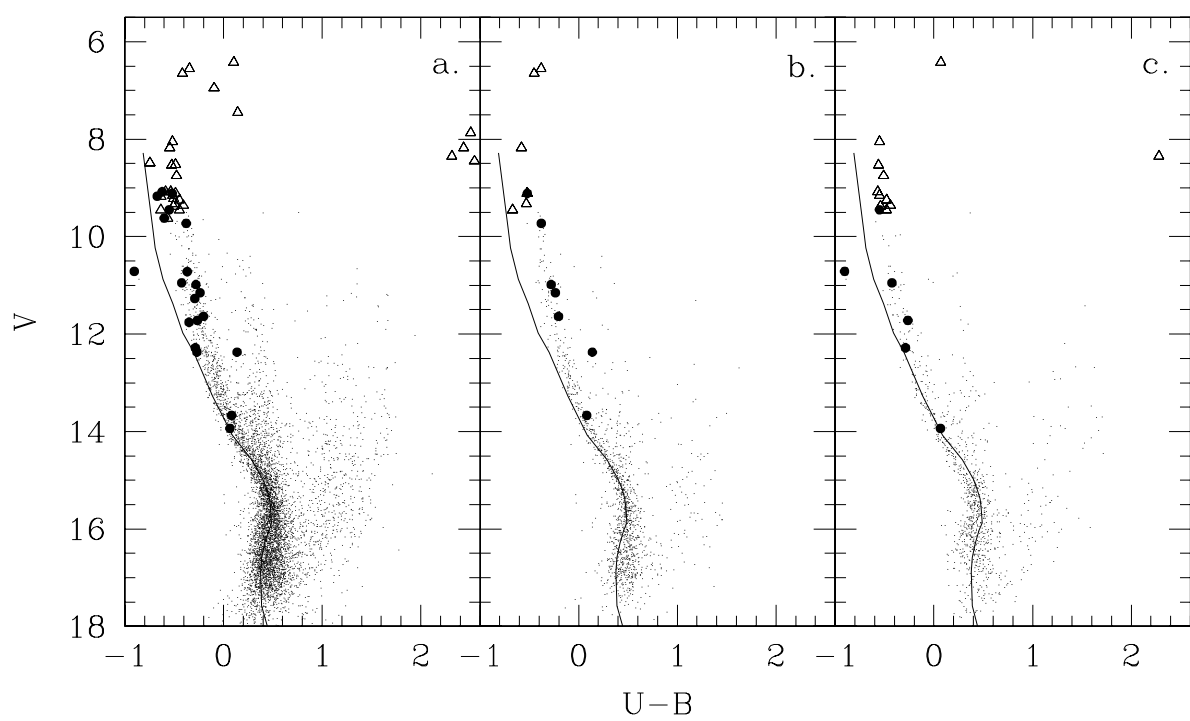


Fig. 4. | V, U-B diagram .

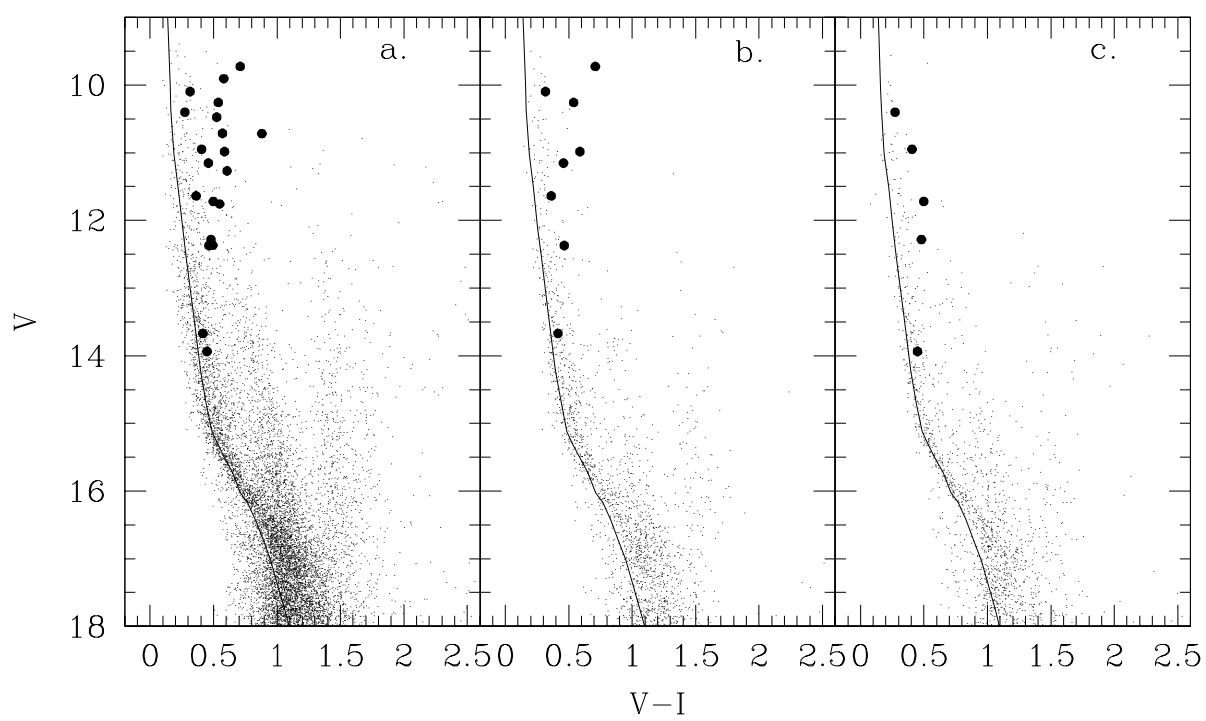


Fig. 5. | V, V-I diagram.

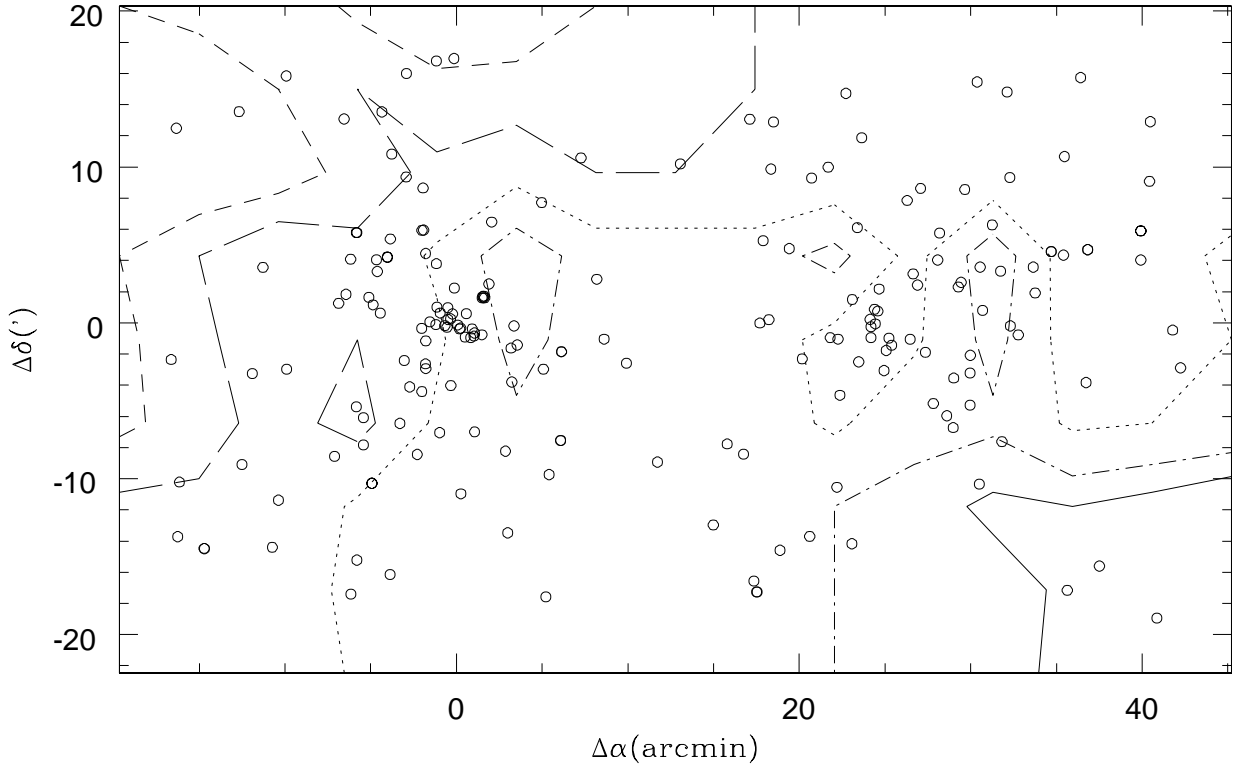


Fig. 6. | Reddening distribution in the vicinity of h & Persei. Positions relative to the center of h Persei at 02:19:00 + 57:09:00 (J2000). The 100 brightest objects are superimposed. The solid, dot-dashed, dotted, long-dashed and dashed lines are respectively $E(B-V) = 0.65, 0.60, 0.55, 0.50$ and 0.45 .

ID	x	y	V	U	B	B	V	V	V	I	V	H	O ost. ID
100	2184.388	944.050	10.380	-0.314	0.464	0.464	0.412	0.412	0.412	-2.822	-2.822	-2.822	2794
101	2203.848	-229.542	10.475	...	0.414	0.414	0.526	0.526	0.526	-1.605	-1.605	-1.605	2804
102	171.524	-493.646	10.400	0.236	0.523	0.523	0.453	0.453	0.453	-2.786	-2.786	-2.786	1242
103	324.182	-584.171	10.443	-0.411	0.261	0.261	0.144	0.144	0.144	-2.823	-2.823	-2.823	1391
104	-56.437	38.175	10.477	-0.387	0.310	0.310	0.232	0.232	0.232	-2.845	-2.845	-2.845	936
105	1109.442	772.894	10.470	0.110	0.567	0.567	0.443	0.443	0.443	-2.774	-2.774	-2.774	1932

Table 2: Photometric data. Table 2 is presented in its entirety in the electronic edition of the Astronomical Journal. A portion is shown here for guidance regarding its form and content.

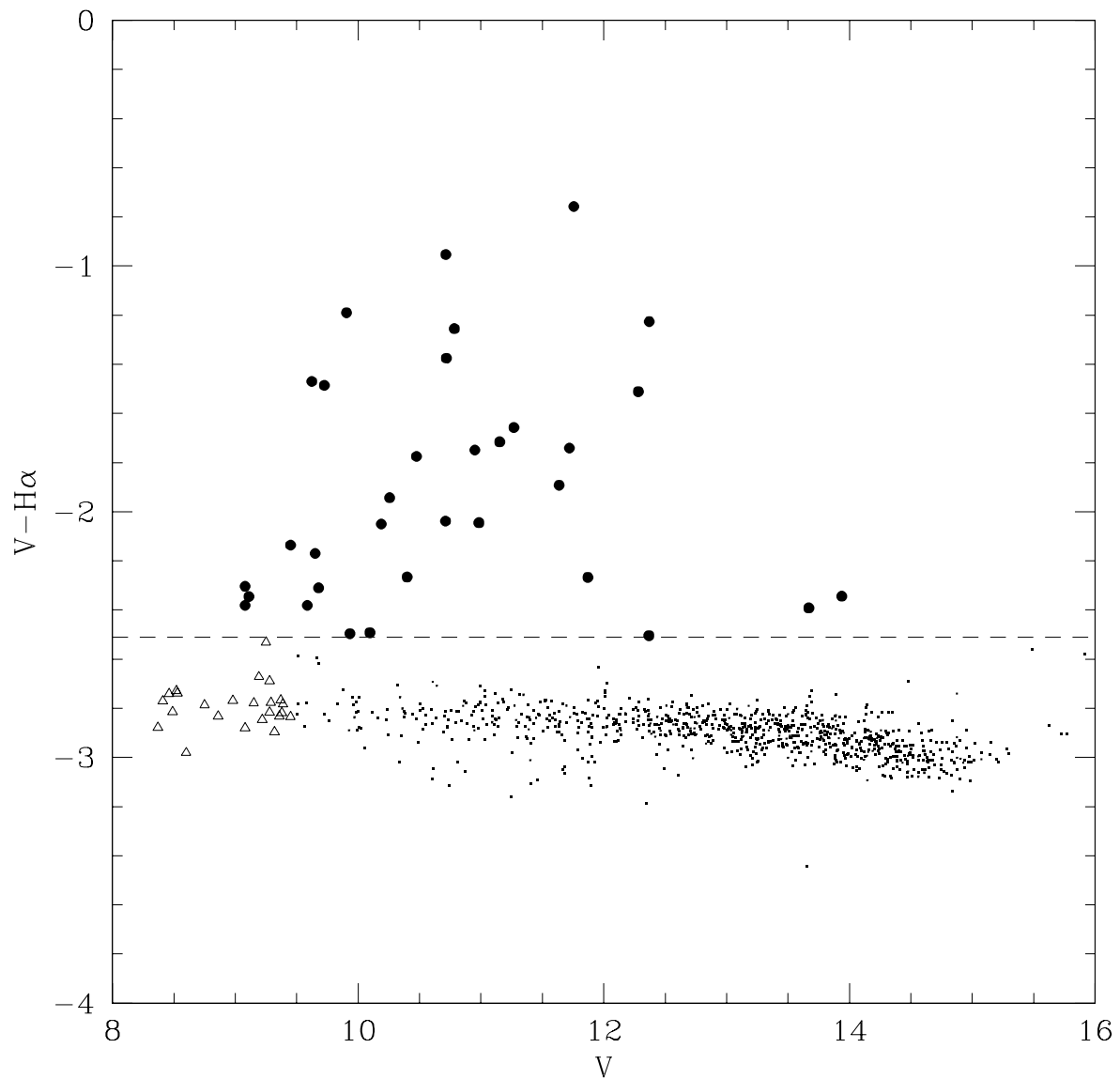


Fig. 7. | $V, V - H\alpha$ Color-Magnitude diagram. Those objects above the dashed line show significant H α emission.

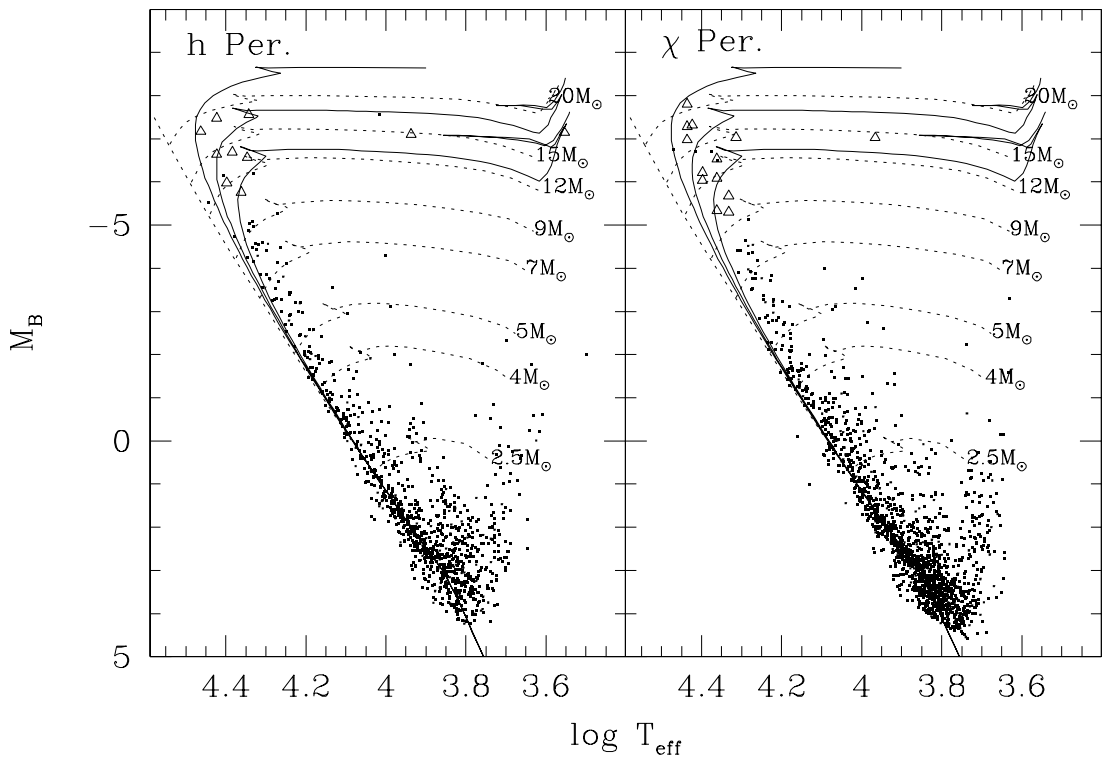


Fig. 8. The H-R diagram of h and χ Persei. The empty triangles are points derived from spectral types. The population of Be stars is excluded from this figure together with those stars with membership probabilities of less than 20% (Mumtaz 1983). Isochrones (solid lines) are shown for $\log \text{age}(\text{yr}) = 6.8, 7.0 \& 7.2$.

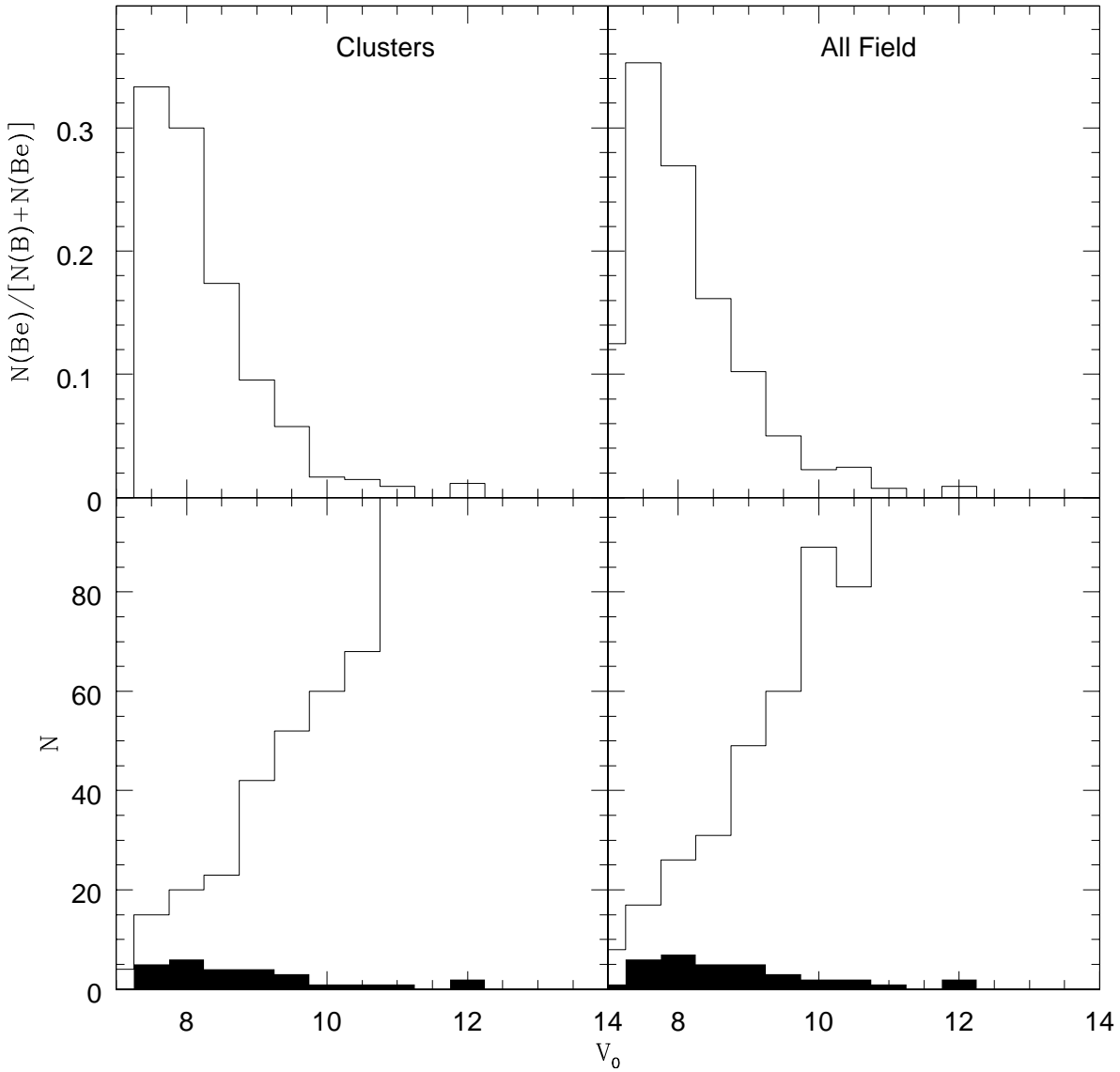


Fig. 9.1 Top panel shows the fraction of Be star to total stars within the cluster population and the entire field. Bottom panel shows the number of B and Be (shaded) stars within both regions.

Author	Method	V	n _{tot}	(B V)	(U B)
Johnson & Morgan (1955)	photoelectric	0.009	0.068	76	0.000 0.053 0.005 0.076
Wildey (1964)	photographic	0.16	0.38	243	0.03 0.11 0.00 0.18
Moat & Vogt (1974)	photographic	0.01	0.08	1437	0.02 0.14 0.03 0.17
Krzesinski et al. (1997)	CCD	0.023	0.061	202	0.041 0.087 0.050 0.057
Krzesinski et al. (1999)	CCD	0.001	0.063	68	0.017 0.059 0.025 0.12

Table 3: Comparison with previous photometric studies. is in the sense of previous study minus the value of obtained in the present study.

ID	x	y	V	U	B	B	V	V	I	V	H	O ost.	ID
28	1363.207	883.212	9.080	-0.620	0.490	-2.304	2138		
29	-120.888	-264.748	9.110	-0.520	0.380	-2.345	847		
31	-644.392	-864.324	9.170	-0.670	0.160	-1.923	309		
42	201.864	-11.658	9.370	...	0.380	-2.466	1268		
45	1308.504	-56.666	9.450	-0.550	0.320	-2.136	2088		
54	1301.495	599.813	9.587	...	0.039	-2.381	2079		
55	-881.546	-869.430	9.620	-0.600	0.220	-2.419	146		
56	784.349	611.905	9.650	...	0.320	-2.170	1702		
58	1624.853	517.354	9.678	...	0.558	-2.310	2402		
60	1496.850	-183.588	9.694	-0.512	0.425	-1.744	2284		
62	193.788	-227.629	9.725	-0.378	0.474	0.709	-1.486	1261		
66	1100.835	591.965	9.905	...	0.493	0.580	-1.190	1926		
68	-114.916	357.033	9.934	...	0.357	-2.496	846		
78	-386.925	110.086	10.096	...	0.280	0.316	-2.492	517		
82	1385.516	89.806	10.189	-0.563	0.319	-2.050	2165		
88	89.547	-45.684	10.257	...	0.454	0.538	-1.943	1161		
91	1966.636	-45.877	10.399	...	0.295	0.273	-2.266	2649		
101	2203.848	-229.542	10.475	...	0.414	0.526	-1.775	2804		
126	1833.016	214.942	10.712	-0.621	0.623	-2.038	2566		
132	1830.679	-620.322	10.714	...	0.454	0.571	-0.953	2563		
137	2128.076	640.403	10.718	-0.366	0.689	0.881	-1.205	2759		
149	1463.242	51.723	10.950	-0.424	0.338	0.406	-1.749	2242		
163	212.904	-85.200	10.984	-0.278	0.580	0.587	-2.045	1282		
191	367.814	-110.785	11.152	-0.237	0.475	0.458	-1.716	...		
209	2151.376	902.980	11.268	-0.291	0.538	0.606	-1.657	2771		
273	214.032	174.599	11.637	-0.203	0.447	0.362	-1.892	1278		
279	1316.548	142.873	11.720	-0.264	0.427	0.498	-1.741	2091		
285	-502.380	-1023.390	11.756	-0.349	0.415	0.548	-0.758	420		
381	1157.409	202.441	12.281	-0.286	0.392	0.480	-1.551	1977		
409	47.680	-280.088	12.370	0.138	0.433	0.464	-1.226	1114		
416	1904.465	913.611	12.368	-0.268	0.502	0.494	-2.504	2600		
964	18.442	11.566	13.669	0.083	0.483	0.416	-2.392	1058		
1199	1081.700	423.908	13.938	0.066	0.480	0.449	-2.344	1912		

Table 4: Be stars detected within the field of the Persei